# Anions Tuned Solid Electrolyte Interphase in Lithium-Ion Batteries

Shi-You Li,*[a, b] Fei Xu,[a] Ning-Shuang Zhang,[a] Peng Wang,[a] and Jie Wang[a]

It is a key and challenging problem to study how the lithium salt anion affects the solid electrolyte interphase (SEI) film formation process. However, the current research focuses on the solvation structure of electrolytes with a general considered conclusion of the preferential reduction effect of anions, while the action mechanism of anions on the solvation structure is rarely studied. Herein, the specific role of anions in the SEI film formation process is illustrated by comparing the influence of anions on the solvation structure with two kinds of boron containing lithium salts. It is found that lithium salt anions can affect the coordination capability of lithium ions and solvents, and then affect the energy consumption in the desolvation process of lithium ions and the composition of SEI film. This work provides a method to study the film formation process, which have certain reference and guide significance for the research of electrolyte field.

## 1. Introduction

Lithium-ion batteries (LIBs) have penetrated into all walks of human's life, greatly changing the people's lifestyle.[1a] Electrolyte, as one of the most important components, plays a vital role in transferring lithium ions ($Li^+$) which directly determines the capacity and cycle property of LIBs.[1b] In order to realize the next generation high-performance energy storage system, the electrolyte with good stability and ionic conductivity is urgently required, thus it is very important to investigate the electrolyte.[1c]

At present, most electrolyte studies focus on the relationship between solvation structure and solid electrolyte interphase (SEI) film.[2] It is well known that the solvation structure can affect the component of SEI film.[3a] In the traditional electrolytes, $Li^+$ is surrounded by solvent molecules to form a lithium ion-solvent complex, and anions are excluded from the solvation sheath.[3b] Theoretical calculations show that the lowest unoccupied molecular orbital (LUMO) of the lithium ion-solvent complex is lower than that of the pure solvent, which indicates that the complex formed by lithium ion-solvent is easier to reduce.[4a] This is because that $Li^+$ can easily coordinate with the carbonyl group (C═O) of ester solvent to increase the bond length of C–O with a weakened interaction.[4b] Therefore, the fragile of SEI film shortens the cycle life of battery, which is harmful to the battery.[4c] In order to solve the above problems, high concentration of electrolyte (HCE) is put forward. In HCE, concentration of lithium salt in the electrolyte is increased, and the solvent around lithium ions can be replaced with anions to form a large number of aggregates (AGG) in the electrolyte. The preferential reduction of such AGG solvation structure will produce more inorganic substances, making a more stable and compact SEI film.[5a] However, the HCE also has some disadvantages. The increase of lithium salts content results in the increased viscosity of electrolyte with poor wettability and the decreased ion transport speed. Therefore, researchers have proposed a local high concentration electrolyte (LHCE), by introducing another low polar solvent that cannot dissolve lithium salt into the high concentration electrolyte system. On the whole, LHCE reduces the content of lithium salt, but it doesn't change the solvation structure.[5b] Introducing an inert solvent which can dissolve lithium salts in weakly-solvating electrolyte (WSE) is a new method for HCE and LHCE. The anions compete with the inert solvent.[5c] Because of the weak polarity of inert solvent, the anions occupy the position of the solvent, and finally the solvation structure dominated by AGG is formed. The common denominator of the three electrolyte mechanisms is that, less solvent separated ion pairs (SSIP) but more contact-ion-pair (CIP) and AGG in the electrolyte. Therefore, the salt anions are preferred to be reduced to produce stable SEI film. However, the cost of high concentration electrolyte is higher. Besides, some researchers modified SEI film by adding lithium salt additives.[5d] In a commercial carbonate-based electrolyte, carbonate electrolyte is easy to be oxidized and decomposed under high potential. Lithium trifluoroacetate (LiTFA), a lithium salt additive, is added to regulate the solvation structure due to its C═O bond, which improves coordination capability of the lithium ion and $TFA^-$. The low LUMO value of LiTFA makes it easier to be reduced than the solvent, resulting in more Lithium fluoride (LiF) inorganic substances, which makes the SEI film more stable.[6a] Lithium nitrate ($LiNO_3$) and fluoroethylene carbonate (FEC) were introduced into electrolyte to adjust the solvation structure, and then uniform SEI film with abundant LiF and $LiN_xO_y$ was formed.[6b] These studies have important guidance for the development of electrolyte, but the common

[a] S.-Y. Li, F. Xu, N.-S. Zhang, P. Wang, J. Wang
School of Petrochemical Technology
Lanzhou University of Technology
Lanzhou 730050, China
E-mail: lishiyoulw@163.com
[b] S.-Y. Li
Key Laboratory of Low Carbon Energy and Chemical Engineering of Gansu Province
Lanzhou 730050, China

Supporting information for this article is available on the WWW under https://doi.org/10.1002/batt.202100274

feature of these studies is that the influence of lithium salts anion on solvation structure is ignored, and the specific action mechanism of lithium anion is rarely reported.

Herein, we investigate the important role of anions in the action mechanism of SEI film formation.[7] In lithium borate difluoroxalate/dimethyl-carbonate (LiDFOB/DMC) electrolyte, $DFOB^-$ anion weakens the coordination ability of $Li^+$ and DMC ($Li^+$-DMC), which makes it easier to desolvate. During the discharge process, the SEI film produced by the preferential reduction of $DFOB^-$ anion is compact and stable. So, it inhibits $Li^+$-DMC co-insertion into graphite and reduces the exfoliation of graphite anode. The lithium tetrafluoroborate/DMC ($LiBF_4$/DMC) electrolyte shows the opposite result. This work provides reference method for the design of SEI film.

## 2. Results and Discussion

The migration of $Li^+$ at the interface composed of graphite anode and electrolyte can be roughly divided into three processes: 1) diffusion of solvated $Li^+$ in electrolyte; 2) $Li^+$ migration in electrolyte toward graphite anode surface; 3) $Li^+$ desolvation from electrolyte at the SEI film on graphite. We will analyze the role of anions in the three stages in detail.[8]

To verify our conclusion, we collected experimental data of Raman and electrospray ionization mass spectrometry (ESI-MS) and carried out simulations on various $Li^+$-solvent interactions in 0.7 M $LiBF_4$/DMC and LiDFOB/DMC (Figure 1). Peaks at 930, 1460, 1755, 2969 and 2884 $cm^{-1}$ are the stretching vibration peak of C–O–C ($U_{C-O-C}$), swinging bending vibration peak of $-O-CH_3$ ($\delta_{C-H}$), stretching vibration peak of –C=O– ($U_{C=O}$), contrastive stretching vibration of C–H ($U_{C-H}$), and symmetric stretching vibration of C–H ($U_{C-H}$), respectively.[9a] The highly electronegative oxygen atom can induce coordination between $Li^+$ and DMC. In Figure 1(a), peaks of $LiBF_4$/DMC and LiDFOB/DMC are significantly different in 1460 $cm^{-1}$ (marked as ♣) and 1755 $cm^{-1}$ (marked as ♠).[9b] Local magnification of Raman in Figure 1(b) shows that the wavenumbers of C=O in $LiBF_4$/DMC and LiDFOB/DMC increase, the wavelength decreases, and the phenomenon of blue shift occurs. The solvation structure around $Li^+$ in a carbonate solvent is an important factor for the performance of LIBs, and the coordination of $Li^+$ and DMC was explained by observing the stretching vibration of $Li^+$ and C=O, indicating that the solvation strength of $LiBF_4$/DMC electrolyte is stronger than LiDFOB/DMC. Generally speaking, the stronger the coordination ability of $Li^+$ with the solvent, the more difficult the desolvation becomes. Thus, it is more difficult for $LiBF_4$/DMC to be desolvated.[9c]

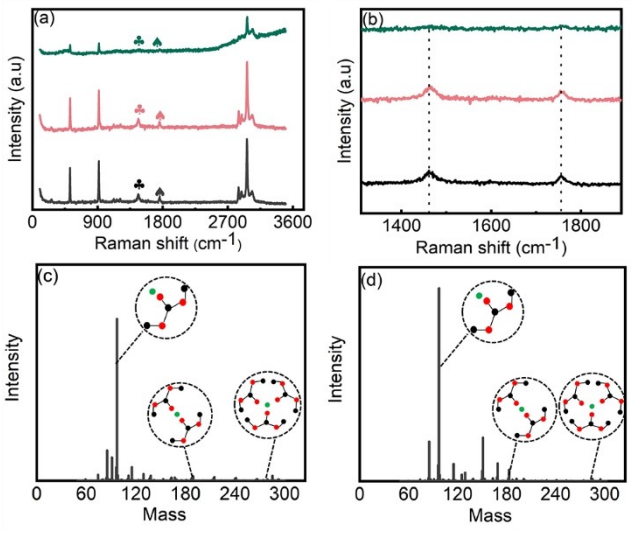


**Figure 1.** a) Raman spectra of different solutions; b) local magnification of Raman (black: DMC, red: $LiBF_4$/DMC, green: LiDFOB/DMC); ESI-MS spectra of c) 0.7 M $LiBF_4$/DMC and d) 0.7 M LiDFOB/DMC.

Raman spectra show that $DFOB^-$ would affect the coordination ability between $Li^+$-DMC, and ESI-MS was used to further determine the solvents molecules numbers around $Li^+$. Although ESI-MS was used as a quantitative tool to reveal the distribution of solvent molecules around $Li^+$, it is important to note that the cationic complexes detected by ESI-MS have actually undergone partial dissolution during flight under the electric field, and therefore, these charged substances do not fully reflect the exact solvation sheaths in the electrolyte. The peaks shown in the mass spectrogram represent the most stable solvation species that should occur in an electrolyte .[10a] Herein, 0.1% formic acid water and 0.1% formic acid acetonitrile were selected as diluent. After analysis, pronounced peaks at mass-charge ratios (*m*/*e*) of 97, 187 and 277 correspond to $[Li(DMC)]^+$, $[Li(DMC)_2]^+$, $[Li(DMC)_3]^+$. The remaining peak is the complex formed by the coordination of $Li^+$ and diluent, which does not affect the coordination of $Li^+$ -DMC. It can be seen from the ESI-MS that the distribution of solvent molecules around the $Li^+$ in $LiBF_4$/DMC and LiDFOB/DMC is similar.[10b] The negative spectrum of $LiBF_4$/DMC and LiDFOB/DMC is shown in Figure S1.

Furthermore, the high coordination capability and dense stacking form of LiDFOB/DMC compared to those of $LiBF_4$/DMC are demonstrated by the radial distribution function (RDF) of $Li^+$ to oxygen, in which LiDFOB/DMC has a higher frequency around $Li^+$ compared to $LiBF_4$/DMC.

The influence of anions on the solvation structure was further studied by RDF, Figure 2(a) shows a snapshot of the molecular dynamic simulation of $LiBF_4$/DMC and LiDFOB/DMC. RDF enables quantification of molecular configurations in a mixture of various atoms and ions in the electrolyte.[11a] The RDF of Li–O pair displays that the solvation structure of the system is the mode of $Li^+$ surrounded by DMC molecules. In the presence of DMC, the $LiBF_4$ salt dissociates and forms $Li^+$ and $BF_4^-$ which are solvated by the DMC molecules. $Li^+$ will preferentially coordinate with the carbonyl oxygen in the DMC solvent because of the electronegative of the oxygen atom on the carbonyl group.[11b] Hence, the RDF of Li–O is commonly used to characterize the DMC solvation shell around the $Li^+$ ion. In $LiBF_4$/DMC electrolyte, $Li^+$ is surrounded by two layers of solvation structure. We focus on the distance between Li and O. As can be seen from Figure 2(b), the position of the first peak appears at 2.045 Å.[11c] In the $LiBF_4$/DMC electrolyte, the coordination ability of $Li^+$ and $O_{DMC}$ was greater than that of

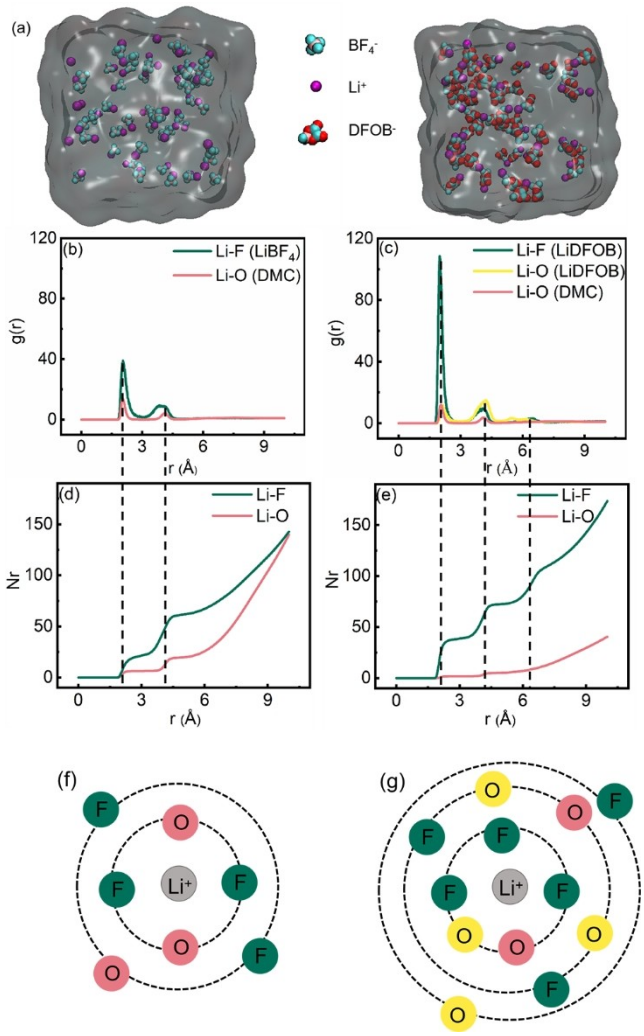


**Figure 2.** a) Snapshots of the MD simulation boxes of $LiBF_4$/DMC and LiDFOB/DMC electrolyte; MD simulation of Li–O and Li–F radical distribution functions *g*(*r*): b) in $LiBF_4$/DMC electrolyte, c) in LiDFOB/DMC electrolyte; d, e) the cumulative coordination number of Li–O, Li–F; f, g) schematic illustration of the radial distribution of $LiBF_4$/DMC and LiDFOB/DMC.

LiDFOB/DMC, indicating that $Li^+$ coordinated with more DMC solvent molecules. In the LiDFOB/DMC electrolyte, $Li^+$ is surrounded by three layers of solvation structure. $DFOB^-$ also participated in the first solvation sheath, by replacing part of the DMC solvent, as shown in Figure 2(c).

The second peak appears at the position of 4.135 Å, implying that the coordination ability of $Li^+$-$O_{DMC}$ in $LiBF_4$/DMC and LiDFOB/DMC electrolyte in the second solvation sheath is basically the same, but the coordination situation of $Li^+$ and anion is different.[12a] In LiDFOB/DMC, there are more anions involved in the second solvation sheath than that in $LiBF_4$/DMC, as shown in Figure 2(b and c). The specific structure of the solvation sheath is shown in Table S1 in the Supporting Information. By calculating the cumulative coordination number ($N_r$) of Li–$O_{DMC}$, it is obvious that $N_r$ in $LiBF_4$/DMC electrolyte is significantly higher than that in LiDFOB/DMC electrolyte, which indicates that $DFOB^-$ anion weakens the coordination ability of $Li^+$ and solvent DMC, making the desolvation of $Li^+$ much easier.[12b] The plateau in the Nr around 2.045 Å indicates the coordination number of $O_{DMC}$ atoms and $O_{DFOB-}$ present in the first solvation shell. It can be seen that in LiDFOB/DMC, $DFOB^-$ also participates in the solvation structure, which weakens the coordination ability of $Li^+$-DMC, as shown in Figure 2(d and e). The RDF schemes between Li and O, F atoms in DMC solvent, the $BF_4^-$ and $DFOB^-$ anion based on the MD simulation are summarized in Figure 2(f and g).[12c]

$Li^+$ is more closely coordinated with DMC in $LiBF_4$/DMC, but less closely coordinated with DMC in LiDFOB/DMC. It shows that different anions will produce different solvation structures, which corresponds to Raman spectra in Figure 1. In $LiBF_4$/DMC, the strength of the first solvation sheath layer and the second solvation layer produced by $Li^+$-DMC coordination ability is higher than that of LiDFOB/DMC. However, the anions in LiDFOB/DMC participating in the solvation sheath is more than that in $LiBF_4$/DMC. When more $DFOB^-$ enters the solvation sheath, part of DMC will be replaced, indicating that $DFOB^-$ has a greater influence on the solvation structure, and there is a competitive relationship between solvent and anion. Therefore, LiDFOB/DMC consumes less energy during desolvation.

From the solvation part, it is found that anions affect the solvation structure, which will inevitably affect the desolvation process (Figure S2).[13a] In LiDFOB/DMC, the SEI film formed by the preferential reduction of $DFOB^-$ is denser than that formed by $BF_4^-$ reduction. In the process of first discharge desolvation, $Li^+$ must remove the carried solvation molecules in order to pass through the compact SEI film. The compact SEI film required higher demand for $Li^+$ desolvation.[13b] The SEI film formed by $LiBF_4$/DMC is relatively loose, and the requirement for $Li^+$ to pass through the SEI film is low. A small part of $Li^+$-DMC may pass through the SEI film together, resulting in the exfoliation of graphite .[13c]

The stronger the coordination capability between $Li^+$ and solvent, the more energy is consumed in the charge transfer process of desolvation. Based on the Arrhenius equation can be deduced to:[14a]

$$\ln\left(\frac{RT}{R_{ct}}\right) = -\Delta G \times \frac{1000}{RT}$$

When plotting 1000/*RT* as the *x*-coordinate and $\ln(RT/R_{ct})$ as the *y*-coordinate, the slope of the straight line gives $-\triangle G$ (kJ $mol^{-1}$). Following this method, the activation energies in the two electrolytes are obtained. According to the relation between $R_{ct}$ and temperature in Arrhenius equation, the activation energies of the charge transfer process in different electrolytes were obtained.[14b] As shown in Figure 3(a), the increased $LiBF_4$/DMC activation energy of the charge transfer process is 73.42 kJ $mol^{-1}$, compared with a lower activation energy of 60.34 kJ $mol^{-1}$ in the LiDFOB/DMC electrolyte. The high activation energy of $LiBF_4$/DMC electrolyte proves that the SEI film generated by the reduction of $BF_4^-$ is unstable, and the strong coordination between $Li^+$ and DMC may be co-inserted in the graphite negative electrode, resulting in its slower reaction kinetics (Figure S3 and Table S2). According to the Tafel plot in Figure 3(b), the current density of $LiBF_4$/DMC

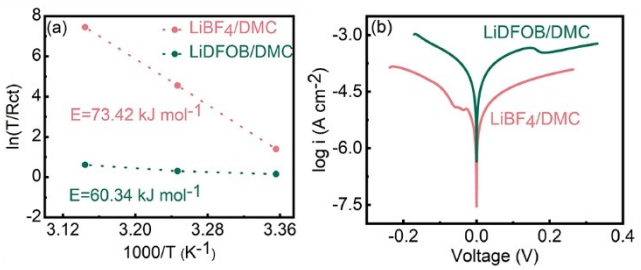


**Figure 3.** a) The activation energies of $R_{ct}$ at different temperatures derived from Nyquist plots; b) Tafel plots in $LiBF_4$/DMC and LiDFOB/DMC.

electrolyte is lower than that of LiDFOB/DMC electrolyte, indicating that in LiDFOB/DMC electrolyte, the SEI film formed by $DFOB^-$ reduction is stable, and desolvation barrier of $Li^+$ decreases, so the kinetic rate of $Li^+$ transport is fast.

Impedance spectroscopy can not only reflect the properties of SEI films, but also provide real-time information about the evolution of SEI film. So, we also use the top view of Nyquist plot in potential-resolved electrochemical impedance spectroscopy (PRI-EIS) to observe the impedance changes at different voltages in situ, as shown in Figure 4.[15a] It can be seen that the SEI film produced by LiDFOB/DMC has a lower impedance, indicating a stable and thin SEI film. It can be clearly seen that the voltage at 1.0 V is the starting point of desolvation, and the

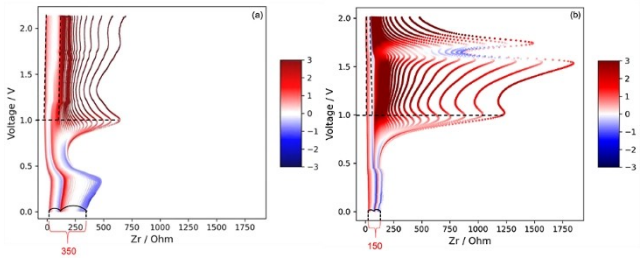


**Figure 4.** The top view of Nyquist plot in potential-resolved electrochemical impedance spectroscopy: a) $LiBF_4$/DMC and b) LiDFOB/DMC.

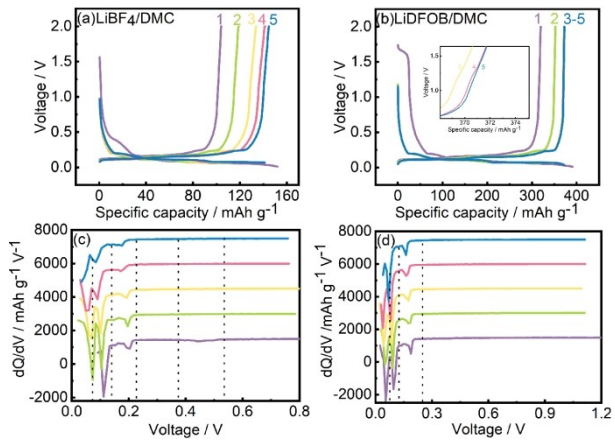


**Figure 5.** The discharging-charging profiles of five times and differential capacity plots after five times discharging of Li/graphite with a, c) $LiBF_4$/DMC and b, d) LiDFOB/DMC.

charge transfer impedance of $LiBF_4$/DMC is significantly larger than that of LiDFOB/DMC, indicating the more energy consumption of $LiBF_4$/DMC during desolvation. Moreover, the DMC solvent molecules around $Li^+$ are hardly to remove, but easily co-inserted with graphite negative electrode.[15b]

From the above two parts, we know that anions will affect the coordination capability between $Li^+$ and solvent, and the SEI film produced by anion reduction will affect the desolvation process. In the following part, we will analyze the effects of different anions on SEI film. We can obviously see that the capacity of LiDFOB/DMC electrolytic is higher than that of $LiBF_4$/DMC, in Figure 5(a and b). Hence, we can guess that the SEI film produced by $DFOB^-$ anion is denser and stable than $BF_4^-$, which can maintain the battery capacity at a higher extent. Figure 5(c and d) shows the differential tolerance curves of $LiBF_4$/DMC and LiDFOB/DMC during the fifth discharge, respectively. From the characteristic peaks of differential tolerance, the cutoff potentials of $LiBF_4$/DMC are 0.55, 0.25, 0.15, 0.05 and 0.01 V, while that of LiDFOB/DMC are 0.60, 0.25, 0.15, 0.05 and 0.01 V, respectively (Figure S4).[16]

The reduction peak in the differential tolerance (d*Q*/d*V*) curve corresponds to the discharge platform in the discharge curve. The positions of these reduction peaks represent the reduction reactions that occur during the discharge process. It is impossible for the reduction reaction to occur at a specific voltage, so we chose the point near each reduction peak as the cutoff voltage in order to observe the change of SEI film with the change of voltage. The impact of different electrolytes on anode morphology evolutions was characterized by the scanning electron microscopy (SEM). In Figure 6, in the middle of the hexagon is the SEM of graphite sheet without cycle in any electrolyte (marked as fresh), Figure 6(a) is the SEM of graphite | Li anode half-cell in $LiBF_4$/DMC electrolyte, disassembled after 8 h of storage, then washed three times using DMC solvent marked as quiescence. Figure 6(b–f) is the SEM

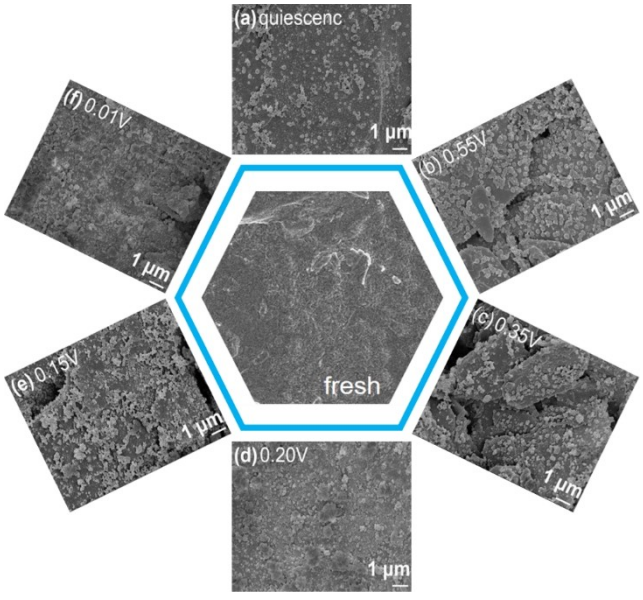


**Figure 6.** SEM of graphite anodes at different voltages in $LiBF_4$/DMC.

images of the half-cell in $LiBF_4$/DMC electrolyte for discharging to 0.55, 0.25, 0.15, 0.05 and 0.01 V, respectively. Obviously, cracks and powders appeared on the graphite surface after the addition of $LiBF_4$/DMC electrolyte, indicating that it was difficult for the instable SEI film formed after the reduction of $BF_4^-$ to inhibit the co-insertion of $Li^+$-DMC. The graphing principle of Figure 7 is the same as that of Figure 6. In Figure 7(a), the SEM of graphite | Li anode half-cell in LiDFOB/DMC electrolyte, treated in the same way as described in Figure 6(a) was tested and marked as quiescence. Figure 7(b–f) shows the SEM diagram with cutoff voltages at 0.60, 0.25, 0.15, 0.05 and 0.01 V in the first discharge process. With the change of voltage after the addition of LiDFOB/DMC, there is no obvious crack on the graphite surface and no powdering phenomenon occurs. Therefore, we believe that the SEI film formed after the preferential reduction of $DFOB^-$ is dense and stable, which can inhibit the co-insertion of $Li^+$-DMC into graphite.[17]

The study of solvation structure shows that $DFOB^-$ weakens the coordination ability of $Li^+$-DMC, so that $DFOB^-$ has the opportunity to enter into the solvation sheath structure to be reduced preferentially during the first discharge process. Compared with $BF_4^-$, the SEI film produced by $DFOB^-$ is more compact and stable with a decreased organic content and the significantly increased inorganic content. The chemical compositions of SEI film were further explored by X-ray Photoelectron Spectroscopy (XPS) to figure out the underlying mechanism.[18a] XPS spectra of $LiBF_4$/DMC electrolyte at different voltages are shown in Figure 8. In the F1s spectrum, the peak with high binding energy belongs to lithium salt $Li_xBF_y$, while the peak with low binding energy corresponds to LiF. With the discharge process, the electrolyte was gradually reduced to produce $Li_xBF_y$ and LiF.[18b] In the C1s and O1s spectra, the C–O bond position are 289.0 and 531.9 eV, while that of C=O are 286.6 and 533.1 eV. In the O1s spectrum, the peak at 530.0 eV is alkyl lithium oxide (ROLi), which is formed by the reduction of the solvent DMC.[18c] In Figure 8, $BF_4^-$ in $LiBF_4$/DMC electrolyte was reduced on the graphite surface, and the inorganic layer formed was unstable and loose. At 0.2 V, $Li^+$-DMC was co-inserted in the graphite layer, resulting in the decomposition of a large number of electrolyte and thickening of the organic layer. Therefore, the content of LiF began to decrease during detection. This phenomenon is consistent with the conclusion of the paper. The SEI film formed by the preferential reduction of $DFOB^-$ anion is relatively stable, so the co-insertion of $Li^+$-DMC into graphite can be inhibited and the capacity of the battery can be maintained at a high level. As can be seen from Figure 8, the content of inorganic substances (LiF) does not increase significantly, which indicates that the SEI film generated by $LiBF_4$/DMC is unstable, resulting in the exfoliation of graphite layer and attenuation of capacity due to the $Li^+$-DMC co-insertion in graphite negative electrode.[18d]

The content of inorganic substances LiF, lithium oxide ($Li_2O$), Lithium metaborate ($LiBO_2$) in the electrolyte of LiDFOB/DMC increased obviously, indicating that the SEI film formed by LiDFOB/DMC was compact and stable with uniform distribution of LiF and $Li_2O$ (Figure 9).[19a] During the desolvation process, the co-insertion of $Li^+$-DMC and the exfoliation of graphite layer was inhibited, and the capacity retention rate was high.[19b]

It is found that the unstable SEI film produced by $BF_4^-$ anion is derived from the strong interactions of $Li^+$-DMC, so $Li^+$-DMC complexes can still penetrate through the SEI film and co-insertion into graphite.[20a] In LiDFOB/DMC electrolyte, the dense and stable SEI film that force $Li^+$ to undergo desolvation, which results in the reversible $Li^+$ intercalation and well-preserved graphite structure.[20b] The mechanism is shown in Figure 10.

## 3. Conclusions

In this study, the structure of the lithium salt anion will affect the solvation structure of the electrolyte, and then affect the desolvation process as well as influence the SEI film. Intriguingly, $DFOB^-$ can weaken the strong coordination capability of $Li^+$-DMC and participate in building the solvation sheath by superseding some DMC molecules. As a result, the electrolyte presents a katabatic energy depletion of $Li^+$ de-solvation. Moreover, $DFOB^-$ can be reduced to LiF and $Li_2O$ preferentially, which is beneficial to form a much stable SEI film with these reduction products. Such SEI film restrains $Li^+$-DMC co-insertion into the graphite anode effectively and reduces the damage to the graphite anode, which is conducive to the faster ion transfer kinetics. This work focuses on exploring what role does the anions play in the process of $Li^+$ solvation sheath and in tunning the composition of SEI film. More than that, the results also provide us with a new idea in constructing a more stable SEI film. In the future, we aim to apply this insight to high and low temperature electrolytes.

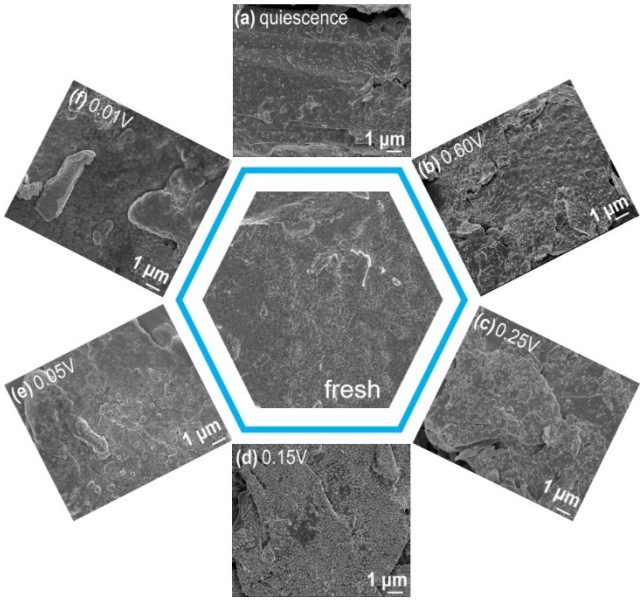


**Figure 7.** SEM of graphite anodes at different voltages in LiDFOB/DMC.

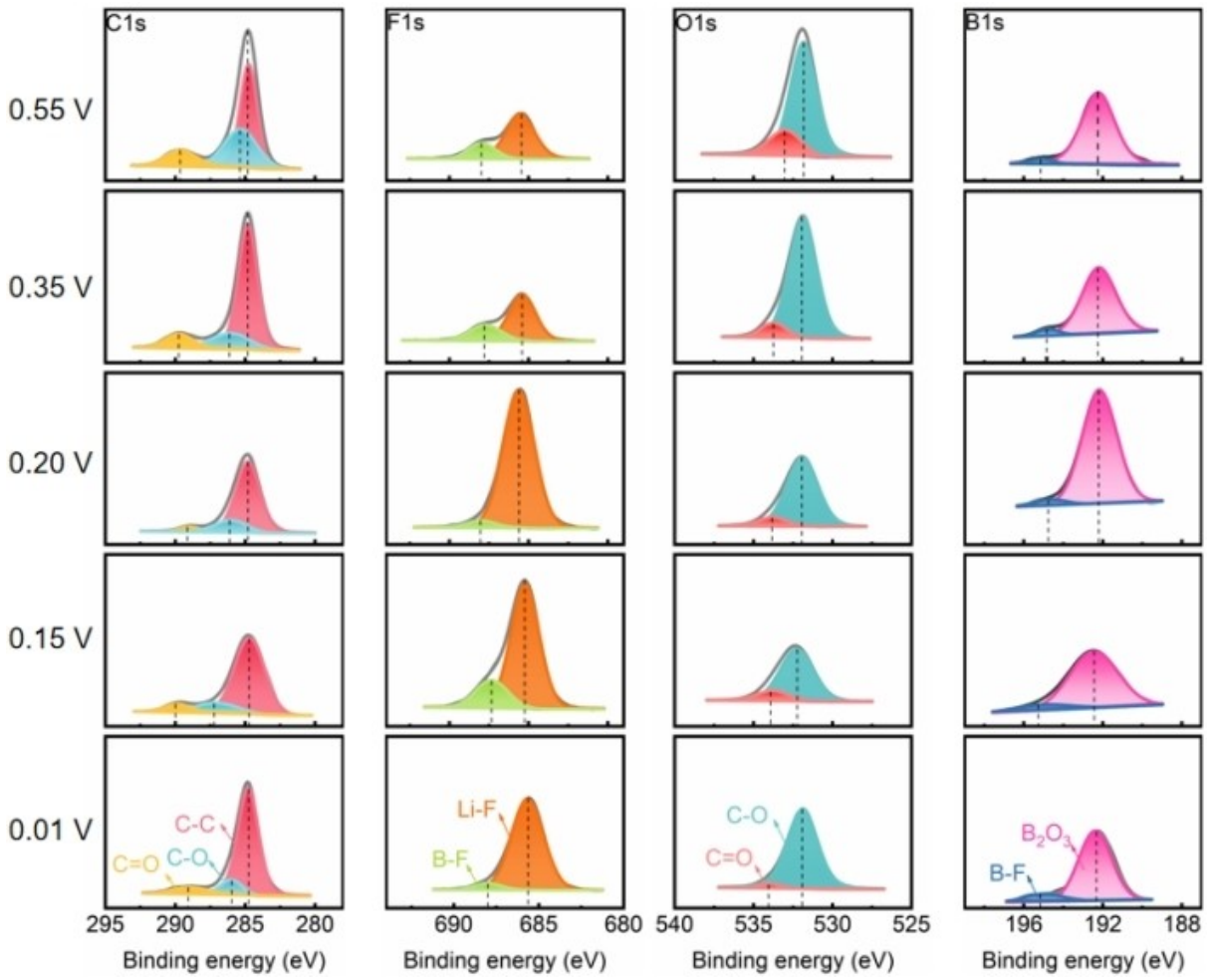


**Figure 8.** XPS of $LiBF_4$/DMC electrolyte at different potentials.

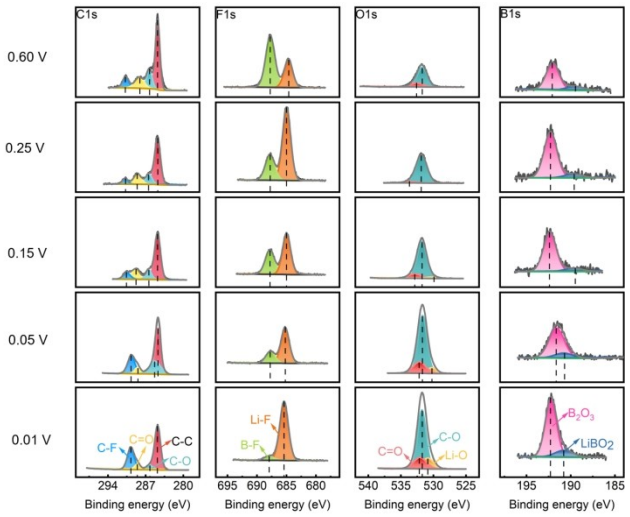


**Figure 9.** XPS of LiDFOB/DMC electrolyte at different potentials.

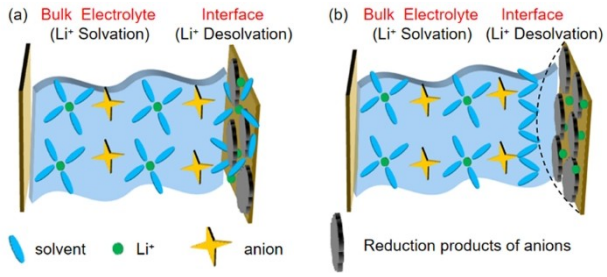


**Figure 10.** Study on the process of $Li^+$ migration at the SEI film: a) $Li^+$-solvent co-insertion in $LiBF_4$/DMC; b) successful $Li^+$ desolvation leading to $Li^+$ intercalation at the graphite anode in LiDFOB/DMC.

## Experimental Section

### Experimental details

$LiBF_4$, Lithium borate disoxalate (LiBOB) and LiDFOB were chosen to investigate in this work due to some common properties of them. However, LiBOB was excluded in the initial experiment because compatibility between 0.7 M LiBOB/DMC electrolyte and graphite is poor. Therefore, $LiBF_4$/DMC and LiDFOB/DMC were retained in the later experiments. $LiBF_4$, LiDFOB and DMC were purchased from Guangdong Canrd New Energy Technology Co.,

Ltd. These reagents were all LIBs grade and used without further purification. A certain amount of $LiBF_4$ and LiDFOB were added to DMC to prepare electrolyte in an Ar-filled glovebox. Graphite powders were provided from Tianjin Aiweixin Chemical Technology Co., Ltd. The graphite electrode slurry (including graphite, acetylene black and polyvinylidene fluoride at a mass ratio of 8:1:1, respectively) was uniformly coated on a copper current collector with a 100 μm doctor blade and dried at 120 °C under vacuum for 12 h. A CR 2025 Li/graphite half cells were assembled in a glovebox with graphite as the working electrode, lithium sheet as the counter electrode and reference electrode, and the Celgard 2400 membrane as separator. 40 μL electrolyte was added to each half cell. The battery testing was performed on the LAND CT2001 A tester (Wuhan LAND Electronics Co., Ltd.), with the voltage range of 2–0.01 V.[21] The electrochemical impedance spectrum (EIS) tests were carried out on the DH7006 electrochemical workstation (Donghua Testing Technology Co., Ltd.). AC-Impedances were tested at 25 °C, 35 °C, 45 °C and 55 °C, respectively, with a frequency range of 10 MHz–0.1 Hz and an amplitude of 5 mV after six times of discharge. In addition, Tafel plots was obtained with a scan rate of 0.25 mV $s^{-1}$ in a quasi-static process.

### Test characterization details

A LabRAM HR Evolution spectrometer (Raman, HORIBA Jobin Yvon S.A.S.) was used to obtain spectra of the electrolyte. The spectral range of Raman is from 100 to 4000 $cm^{-1}$. The molecular ion pairs ionized from the electrolyte were measured by ESI-MS (Thermo Scientific Q Exactive). Formic acid and formic acid acetonitrile were added into $LiBF_4$/DMC (or LiDFOB/DMC) electrolyte to prepare sample. The sample is elect"ropositive as inflicting a relative high DC voltage on the nozzle. After the fully dissolution of $LiBF_4$ and LiDFOB in DMC, 0.5 mL solution was taken for testing, by the way, whether lithium salt has fully dissolved in the solvent has a great impact on the test process. In order to study the situation of graphite electrode under different cutoff voltage during the discharge process, the battery was disassembled in the glovebox. Then the negative electrode was taken out and rinsed with DMC for 3 times, and then tested after drying. The surface elements of SEI films at different voltage after initial discharge were analyzed by XPS (GG314-JPS-9200). In addition, the morphologies of the electrode were analyzed by SEM (JSM-6100) at different cutoff voltage.

### Calculation details

Gaussian 09 software and B3LYP/6-31G+ (d, p) basis set were used for structural optimization. The molecular dynamics simulations (MD) were conducted using GROMACS 2019. 6. It is calculated that there were 893 DMC solvent molecules, 53 $LiBF_4$ and 53 LiDFOB molecules in every 0.7 M electrolytic liquid system, so the size of the solvation box was set as 5 ×5×5 Å with a density of DMC (1.069 g/$cm^3$, $T=298$ K and $P=1$ atm).[22a] Further, the packing optimization for molecular dynamics simulations (PACKMOL) were utilized to generate the initial configuration of $LiBF_4$/DMC and LiDFOB/DMC system. The force field of OPLS-AA and the Mulliken charge was used. Firstly, the system was allowed to evolve under NVT conditions (up to 100 ps) to prebalance the system from its initial configuration. Further annealing simulation at constant NPT conditions (0–300 K) for 100 ps was carried out. Later, the system was simulated under NVT conditions for 20 ns. Both the mean square displacement (MSD) and RDF was calculated through Gromacs built-in programs.[22b]

## Conflict of Interest

The authors declare no conflict of interest.

**Keywords:** The authors would like to thank Gansu Provincial Department of Education: Industrial Support Program Project (2021CYZC-18); Gansu Province Science and Technology Planning Project (20JR5RA469); Lanzhou University of Technology hongliu first-class discipline construction program.

[1] a) C. Yan, R. Xu, Y. Xiao, J. Ding, L. Xu, B. Li, J. Huang, *Adv. Funct. Mater.* **2020**, *30*, 1909887; b) J. Zheng, J. A. Lochala, A. Kwok, Z. Deng, J. Xiao, *Adv. Sci.* **2017**, *4*, 1700032; c) L. Liang, X. Li, F. Zhao, J. Zhang, Y. Liu, L. Hou, C. Yuan, *Adv. Energy Mater.* **2021**, *11*, 2170079.
[2] D. Zhao, J. Wang, H. Lu, P. Wang, H. Liu, S. Li, *J. Power Sources* **2020**, *456*, 228006.
[3] a) J. Ming, Z. Cao, W. Wahyudi, M. L. Liu, P. Kumar, Y. Q. Wu, *ACS Energy Lett.* **2018**, *3*, 335–340; b) K. Xu, *J. Electrochem. Soc.* **2007**, *154*, A162.
[4] a) X. Chen, H. R. Li, X. Shen, Q. Zhang, *Batteries & Supercaps* **2019**, *2*, 1–5; b) X. Chen, H. R. Li, X. Shen, Q. Zhang, *Angew. Chem. Int. Ed.* **2018**, *57*, 16572; c) X. Zhang, X. Chen, X. Cheng, B. Li, X. Shen, C. Yan, J. Huang, Q. Zhang, *Angew. Chem.* **2018**, *130*, 5399–5403; *Angew. Chem. Int. Ed.* **2018**, *57*, 5301–5305.
[5] a) Y. Yamada, K. Furukawa, K. Sodeyama, K. Kikuchi, M. Yaegashi, Y. Tateyama, A. Yamada, *J. Am. Chem. Soc.* **2014**, *136*, 5039–5046; b) L. Yu, S. Chen, H. Lee, L. C. Zhang, M. H. Engelhard, Q. Y. Li, S. H. Jiao, J. Lin, W. Xu, J. G. Zhang, *ACS Energy Lett.* **2018**, *3*, 2059–2067; c) Y. Yu, X. Chen, C. Yan, X. Zhang, W. Cai, J. Huang, Q. Zhang, *Angew. Chem.* **2020**, *133*, 4136–4143; d) J. Wang, D. Zhao, Y. Cong, N. Zhang, P. Wang, X. Fu, X. Cui, *ACS Appl. Mater. Interfaces* **2021**, *13*, 16939–16951.
[6] a) Z. Wang, F. Qi, L. Yin, C. Sun, B. An, H. Cheng, F. Li, *Adv. Energy Mater.* **2020**, *10*,1903843; b) X. Q. Zhang, X. Chen, L. Hou, B. Li, X. Cheng, J. Huang, Q. Zhang, *ACS Energy Lett.* **2019**, *4*, 411–416.
[7] J. Ming, Z. Cao, W. Wahyudi, M. Li, P. Kumar, Y. Wu, J. Hwang, M. N. Hedhili, Y. Sun, L. Li, *ACS Energy Lett.* **2019**, *4*, 1584–1593.
[8] Q. Li, D. Lu, J. Zheng, S. Jiao, L. Luo, C. Wang, K. Xu, J. Zhang, W. Xu, *ACS Appl. Mater. Interfaces* **2017**, *9*, 42761–42768.
[9] a) M. G. Giorgini, K. Futamatagawa, H. Torii, M. Musso, S. Cerini, *J. Phys. Chem. Lett.* **2015**, *6*, 3296–3302; b) S. K. Jeong, M. Inaba, Y. Iriyama, T. Abe, Z. Ogumi, *Electrochem. Solid-State Lett.* **2003**, *6*, A13; c) H. Nakagawa, Y. Domi, T. Doi, M. Ochida, S. Tsubouchi, T. Yamanaka, T. Abe, Z. Ogumi, *J. Electrochem. Soc.* **2014**, *161*, A480–A485.
[10] a) T. Fukushima, Y. Matsuda, H. Hashimoto, R. Arakawa, *Electrochem. Solid-State Lett.* **2001**, *4*, A127; b) K. Xu, A. W. Cresce, *J. Mater. Res.* **2012**, *116*, 26111–26117; c) C. M. Tenney, R. T. Cygan, *J. Phys. Chem. C* **2013**, *117*, 24673–24684.
[11] a) O. O. Postupna, Y. V. Kolesniket, O. N. Kalugin, O. V. Prezhdo, *J. Phys. Chem. B.* **2011**, *115*, 14563–14571; b) M. T. Ong, O. Verners, E. W. Draeger, A. Duin, V. Lordi, J. E. Pask, *J. Phys. Chem. B.* **2015**, *119*, 1535–1545; c) T. Z. Hou, G. Yang, N. N. Rajput, J. Self, S. W. Park, J. Nanda, K. A. Persson, *Nano Energy* **2019**, *64*, 103881.
[12] a) M. F. He, K. C. Lau, X. D. Ren, N. Xiao, W. D. McCulloch, L. A. Curtiss, Y. Wu, *Angew. Chem. Int. Ed.* **2016**, *5*, 15310–15314; b) X. Cao, P. Gao, X. Ren, L. Zou, M. H. Engelhard, *Proc. Natl. Acad. Sci. USA* **2020**, *118*, e2020357118; c) T. R. Jow, S. A. Delp, J. L. Allen, J. P. Jones, M. C. Smart, *J. Electrochem. Soc.* **2018**, *165*, A361–A367.
[13] a) J. Huang, J. Liu, J. He, M. Wu, S. Qi, H. Wang, F. Li, J. Ma, *Angew. Chem. Int. Ed.* **2021**, *60*, 1–7; b) P. M. Chekushkin, I. S. Merenkov, V. S. Smirbov, S. A. Kislenko, V. A. Nikitina, *Electrochim. Acta* **2021**, *372*, 137843; c) C. Jiang, Y. Gu, Y. Chen, Y. Wu, J. Ma, C. Wang, W. Hu, *ACS Appl. Mater. Interfaces* **2020**, *12*, 10461–10470.
[14] a) K. Xu, A. W. Cresce, *J. Mater. Res.* **2012**, *27*, 2327–2341; b) H. C. Yang, L. C. Yin, H. F. Shi, K. He, H. M. Cheng, F. Li, *Chem. Commun.* **2019**, *55*, 1–3.
[15] a) H. Dong, X. Fu, P. Wang, H. Ding, R. Song, S. Wang, R. Li, S. Li, *Carbon.* **2021**, *173*, 687–695; b) Y. Yamada, Y. Iriyama, T. Abe, Z. Ogumi, *Langmuir* **2009**, *25*, 12766–12770.
[16] S. Li, Y. Li, P. Wang, Z. Li, W. Li, H. Liu, X. Cui, *J. Power Sources* **2020**, *471*, 228426.
[17] T. Pajkossy, R. Jurczakowski, *Curr. Opin. Electrochem.* **2017**, *1*, 53–58.

[18] a) Y. Jie, X. Liu, Z. Lei, S. Wang, Y. Chen, F. Huang, R. Cao, G. Zhang, S. Jiao, *Angew. Chem. Int. Ed.* **2020**, *132*, 3533–3538; b) N. Ehteshami, L. Ibing, L. Stolz, M. Winter, E. Paillard, *J. Power Sources* **2020**, *451*, 227804; c) C. Jcab, A. Tl, *J. Energy Chem.* **2021**, *60*, 178–185; d) X. Ren, P. Gao, *Proc. Nat. Acad. Sci.* **2020**, *117*, 28603–28613.
[19] a) L. Yu, S. Chen, *ACS Energy Lett.* **2018**, *3*, 1–24; b) K. Xu, A. von Cresce, U. Lee, *Langmuir* **2010**, *26*, 11538–11543.
[20] a) C. Sang, X. Kong, *J. Am. Chem. Soc.* **2021**, *143*, 10301–10308; b) W. Wahyudi, V. Ladelta, *Adv. Funct. Mater.* **2021**, *31*, 2101593.
[21] G. Lu, S. Qiu, H. Lv, J. Liu, Y. Bai, *Electrochim. Acta* **2014**, *146*, 249–256.
[22] a) B. Ravikumar, M. Mynam, B. Rai, *J. Phys. Chem. C* **2018**, *122*, 8173–8181; b) A. Cresce, O. Borodi, K. Xu, *J. Phys. Chem. B* **2012**, *116*, 26111–26117.

Manuscript received: September 28, 2021
Revised manuscript received: November 21, 2021
Accepted manuscript online: December 1, 2021
Version of record online: December 14, 2021